https://erjm.journals.ekb.eg
ISSN:

DOI: ---------

ERJ
Engineering Research Journal
Faculty of Engineering
Menoufia University

Performance Investigation of Two Vertical-Axis Twisted Rotor Models

Ali M. Abdelsalam, Ismail M. Sakr, M. Kotb, and Khaled Yousef

Mechanical Power Engineering Department, Faculty of Engineering, Menoufia University, Shebin El-Kom, Egypt.
(Corresponding author: ismailsakr@yahoo.com)

ABSTRACT
The world nowadays is looking for a clean source of renewable energy that produces no air or water pollution. Wind energy has become an optimal solution for world needs and the governments offer great attention to wind-energy development. In the present work, two outstanding Savonius rotor models are first investigated numerically using the three-dimensional unsteady Reynolds-averaged Navier-Stokes (URANS) equations, along with the Shear Stress Transport (SST) *k-ω* turbulence model. Various twist angles are trained for both rotor models and the best efficient model is further fabricated and tested experimentally using an open jet wind tunnel. The numerical and experimental results show good agreement, and the proposed rotor geometry has superior performance. The maximum power coefficient obtained for that optimum rotor is found to be 0.221 at the highest performance twist angle of 45^{o}. Furthermore, the proposed rotor model introduces a positive torque coefficient during the entire rotation cycle, with reduced cyclic torque.

Keywords: *Savonius turbine, twisted blades, optimum rotor, modified profile.*

1. Introduction

The basic role in converting the wind energy into mechanical energy by the wind turbine is the blade shape. Savonius turbine is a simple vertical axis wind turbine suitable for highly turbulent flows that vary considerably in direction [1]. This is the typical case for low power applications in urban environments, as it has a good response to fast changes in wind direction. Detailed reviews exploring the significant parameters dominating the Savonius rotor performance were presented by different authors, see [2, 3].

Several researchers have proposed different shapes of the advancing and returning blades of the Savonius rotor to maximize the power output. In a numerical investigation by Gad et al. [4], a modification process of the Savonius rotor blades was proposed and tested. Two methods were trained for modifying the blade shape. The first method was based on determining nine points on the perimeter of the blade to generate four polynomial shapes. The second method considered V-shape blade rotor with three different V- angles. The influence of the rotor blade modification was checked based on the torque and power coefficients. One of the proposed polynomial blade shapes like a hook had the best performance over the other rotors. Rotors with blades shaped like a hook, have slightly higher moments as the airflow is more directed to the tip of the blades.

Saeed et al. [5] studied numerically different proposed shapes of the rotor blade assuming unsteady two-dimensional flow. In their studies, different turbulence models were compared and the results showed that the realizable *k*-ε turbulence model was the best turbulence model. The blade shape modification has achieved a 23.9% increase in power coefficient (C_P), compared to the classical rotor. Furthermore, the modified rotor without a shaft has achieved a 35.9 % increase in C_P, compared to the classical rotor. In a numerical investigation by Kacprzak et al. [6], comparisons were performed between three geometries of Savonius wind turbine rotors; namely Classical, Bach-type and Elliptical designs. The Elliptical Savonius rotor performed better than both the Bach-type and Classical Savonius rotors in the range of tip speed ratio between 0.2 and 0.4. Al-Ghriybah et al. [7,8] proposed one and two more inner blades along with the advancing and returning blades of the Savonius rotor. Different angles and different values of spacing between inner

blades were investigated. The simulations showed an improvement in the turbine performance of 32.9% in comparison with the conventional Savonius turbine

The behavior of the Savonius rotor is characterized by cyclic torque which causes unfavorable cyclic stress to blade structure (dynamic loads on the turbine blades) [9]. The periodicity in the torque angular distribution has the same number of rotor blades [10]. One solution proposed to overcome this problem is employing a higher number of blades. However, better performance has been shown by two-bladed rotor over rotors with the higher number of blades [11, 12]. Another solution is the multi-stage rotor of staggered stages [13-17]. Moreover, the helical Savonius rotor is further used to reduce the moment oscillation at operation. The helical shape wind turbine is a rotor of infinite stages, with negligible height and lagged one another by angles that tend to 0°. The helical blade is generated by forming at a twist angle (φ) between the upper and lower ends of the rotor blades. They have a relatively lower vibration load due to the helix structure of each blade and vibration is thus balanced off [18]. Helical-type VAWTs produce minimal shadow flicker due to one end of each blade being curved in a helix structure [19].

Oliveira and Petry [20] introduced a 180° twist angle to the rotor blades as a more efficient rotor in terms of power coefficient uniformity with low oscillation behavior. Kamoji et al. [21] examined a helical Savonius rotor with a twist of 90° in an open jet wind tunnel. The results reported a positive static torque coefficient for the helical rotor at all the rotor angles. Further, Damak et al. [22] investigated experimentally the performance of the helical Savonius rotor with a twist of 180^{o}, at different wind speeds of 6, 7.5, 8.8, and 11.1 m/s. The results clearly improved the performance of the helical geometry compared with the conventional geometry. Lee et al. [23] performed a numerical and experimental investigation on helical rotor angles of 0°, 45°, 90°, and 135°. The results revealed that the maximum C_P occurs at a twist angle of 45^{o}. However, the value of C_P at twist angles of 90° and 135° was found to be lower than that at 0°.

El-Askary et al. [24] tested numerically and experimentally the twist of modified blades for the Savonius rotor. Different twist angles were investigated at an overlap ratio (δ) of 0.15 and aspect ratio (AR) of 1. The modified twisted rotor attained in [24] was further optimized in their work [25] at a twist angle of 45^{o} for various values of δ and AR. The numerical results showed a significant improvement for the performance of the twisted modified rotor without overlapping (δ=0) and at AR=2. It is worth noting that, the different research performed on twisted blades confirmed the optimum twist angle is not the same for the different designs. A recent review by Cuevas-Carvajal et al. [26] recommended that twisting the angle of blades should be investigated to further enhance the rotor performance.

Inferring the above studies, two main benefits can be achieved by introducing twist to the modified shapes of rotor blades, which include reduced cyclic torque and improved performance. The blade shape related to the twisted rotor plays the main role in achieving these benefits. The present work conducts experimental and numerical investigations on the performance of two twisted VAWT models, proposed after numerical simulations by Saeed et al. [5] and Saad et al. [25]. In the present study a numerical comparison of the two superior models of the Savonius rotor blades under different geometrical and operational conditions is considered. Then, experimental validation is executed for the best efficient rotor model. For the rest of the paper, the numerical methodology is presented in section 2. The utilized Savonius rotor models are discussed in section 3, while the experimental setup is introduced in detail in section 4. Section 5 introduces the numerical and experimental results and discussion for both rotor models. Finally, the conclusion obtained is presented in section 6.

2. Numerical Methodology

In the current study, ANSYS Fluent 17.0 is used to compute the flow field around the considered wind rotors. The sliding mesh model, will be discussed later, is selected to simulate the unsteady rotor operation, which is demonstrated in Figure (1). The rotation angle and the angular velocity are represented by $\boldsymbol{\theta}$ and Ω, respectively. The computational domain is divided into two zones, the first one is the rotating zone around the rotor and the second is the fixed zone, as shown in Figure (2). The two zones are separated by an interface and the rotating zone is allowed to rotate with different rotational speeds. ANSYS ICEM program has been utilized for the generation of the computational grids. The computational domain is spatially discretized by tetra cells to solve the Unsteady Reynolds-Averaged Navier-Stokes (URANS) equations using finite volume method. The mesh size is carefully adjusted to limit the y+ value to be less than 5. The simulations have been executed on a Dual NVIDIA Quadro P4000, 8GB, 4mDP (7X20T) CPU, Dual Intel Xeon Silver 4114 2.2GHz, 3.0GHz Turbo, 10 C,

9.6GT/s 2UPI, 14M Cache, HT (85W) DDR4-2400 Processor, installed memory (RAM): 96GB (12x8GB) 2666 MHz DDR4.

Uniform velocity is considered as the inlet boundary condition for the domain inlet. The exit of the computational domain, see Figure (2), is taken to be away 15D from the center of the rotor, where D is the rotor diameter. Hence, the outlet boundary is considered as an atmospheric pressure [27]. The turbulence intensity considered in the present computation is taken to be 5% based on our previous work [24]. The top, bottom and lateral sides of the present domain are 5D distance from the center of the rotor, which corresponds to 2 % blockage ratio. These four sides are considered symmetry boundary conditions in the computations.

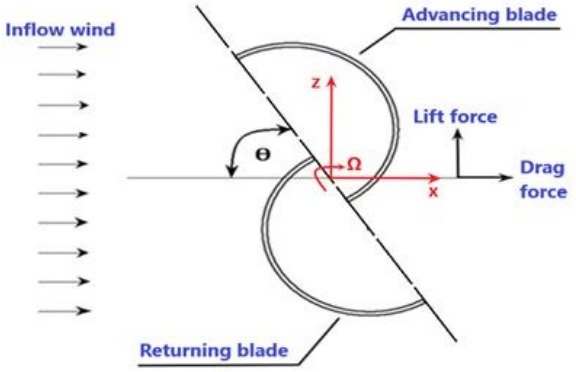

Figure 1- Schematic diagram of the rotor blades

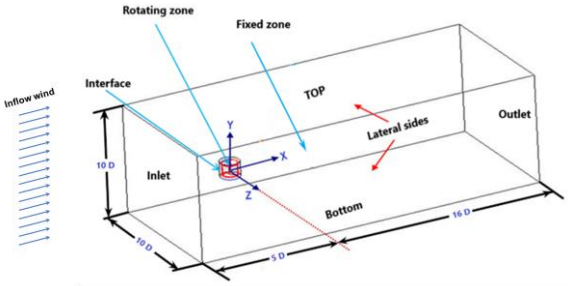

Figure 2- The computational domain (Not to scale)

The general conservation equation formulation for sliding meshes is expressed in Eq. (1).

$$\frac{d}{dt}\int \rho\Phi dV + \int \rho\left(\vec{u}-\vec{u}_g\right).d\vec{A} = \int \nabla\Phi\Gamma.d\vec{A} + \int S_\Phi\, dV \quad (1)$$

where, ρ is the fluid density, Φ is the general scalar represents components of the velocity in the *x, y* and *z* directions, $\vec{u}$ is the flow velocity vector, $\overrightarrow{u_g}$ is the mesh velocity of the moving mesh, Γ is the diffusion coefficient, S_Φ is the source term of Φ.

The governing mass conservation equation is formulated as

$$\nabla.(\vec{u}) = 0 \quad (2)$$

Since the mesh motion in the sliding mesh formulation is rigid, all cells retain their original shape and volume. Consequently, the time rate of change of the cell volume is zero so, $\Delta V^{n+1} = \Delta V^n$ and the unsteady term becomes $\frac{d}{dt}\int \rho\Phi dV = \frac{\left[(\rho\Phi)^{n+1}-(\rho\Phi)^n\right]\Delta V}{\Delta t}$ and the volume time derivative of the control volume becomes zero, this leads to $\int \vec{u}.d\vec{A} = 0$. Since the mesh is moving, this leads to the solutions to Eq. (1) for the sliding mesh motion to be inherently unsteady.

The SST *k-ω* turbulence model is used to close the URANS equations, as recommended in numerous studies [6]. The transport equations for the SST *k–ω* model are formulated as follows ؛

Turbulence kinetic energy *k*-equation:

$$\frac{\partial}{\partial t}(\rho k) + \nabla.\left(\rho k u_i\right) = \nabla.\left[\left(\mu + \frac{\mu_t}{\sigma_k}\right)\nabla k\right] + G_k - Y_k \quad (3)$$

Specific dissipation rate *ω*-equation

$$\frac{\partial}{\partial t}(\rho\omega) + \nabla.\left(\rho\omega u_i\right) = \nabla.\left[\left(\mu + \frac{\mu_t}{\sigma_\omega}\right)\omega\nabla\right] + G_\omega - Y_\omega \quad (4)$$

where, G_k represents the generation of turbulence kinetic energy, Y_k is the dissipation of turbulence kinetic energy, while G_ω refers to the generation of. ω, Y_ω points to the dissipation of ω while σ_k and σ_ω are turbulent Prandtl numbers for k and ω respectively.

The semi-implicit method for pressure-linked equation (SIMPLE) algorithm is used as the link between the pressure and velocity in the calculation domain. The second-order upwind scheme is selected for improving simulation accuracy. The time step size is taken as 0.001 s for all the tip speed ratios with

maximum value of the rotation angle θ=3.6°. The simulations are continued till achieving consistent torque from the rotor with repeated values during the further rotor cycle.

3. Savonius Rotor Models

Two rotor models are first investigated numerically in the present work. The first model, Model 1, is a modified geometry of the optimum rotor presented in [25] which proved superior performance for twisted rotor blades. The second one, Model 2, is a twisted rotor with optimum blade profile adopted based on [5]. For both proposed models, different twist angles are introduced as shown in Figure (3) to fetch the best rotor design. The detailed rotor dimensions, which is kept the same for the two models, are described in Table 1. The blade profile of Model 1 is represented by Eq. (5) while equation (6) represents the blade profile of Model 2.

$$Z = 0.55 + 0.62X - 1.7X^2 + 4.14X^3 - 1.51X^4 - 7.57X^5 \quad (5)$$

$$Z = -101.38 + 1.9X + 0.043X^2 + 0.00064X^3 + 5.891 * 10^{-6}X^4 + 2.0612 * 10^{-8}X^5 \quad (6)$$

where X is measured from the center of the blade

Table 1- Specifications of the present models

Parameter	Model ١/ Model ٢
Rotor diameter, D, mm	٣٠٠
Rotor height, H, mm	٦٠٠
End plate diameter, D_o, mm	٣٣٠
Aspect Ratio, AR	٢.٠
mmδ, Overlap ratio,	٠.٠

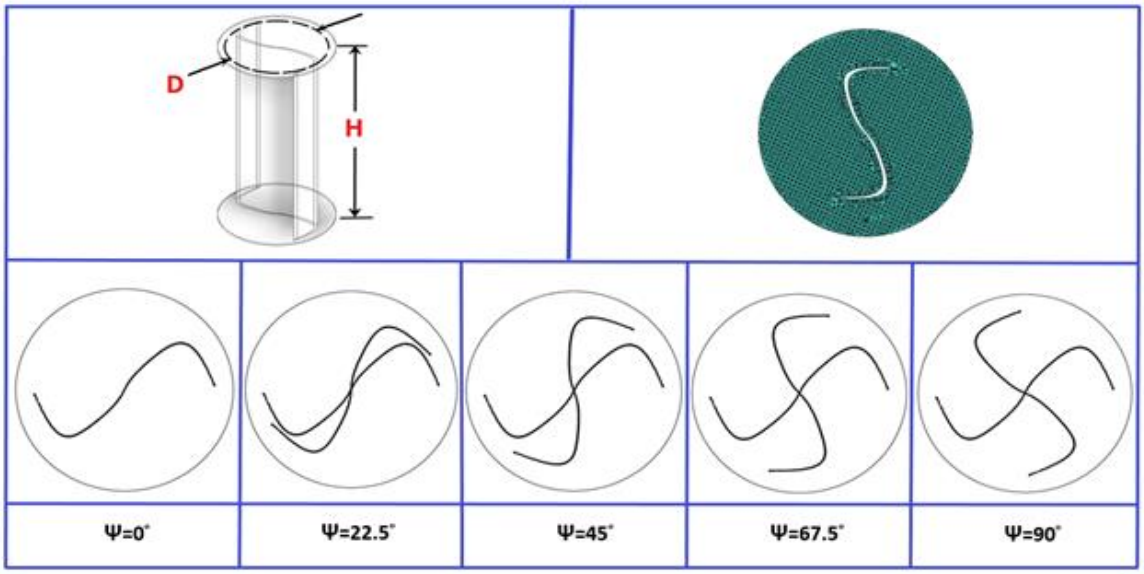

(a) Model 1

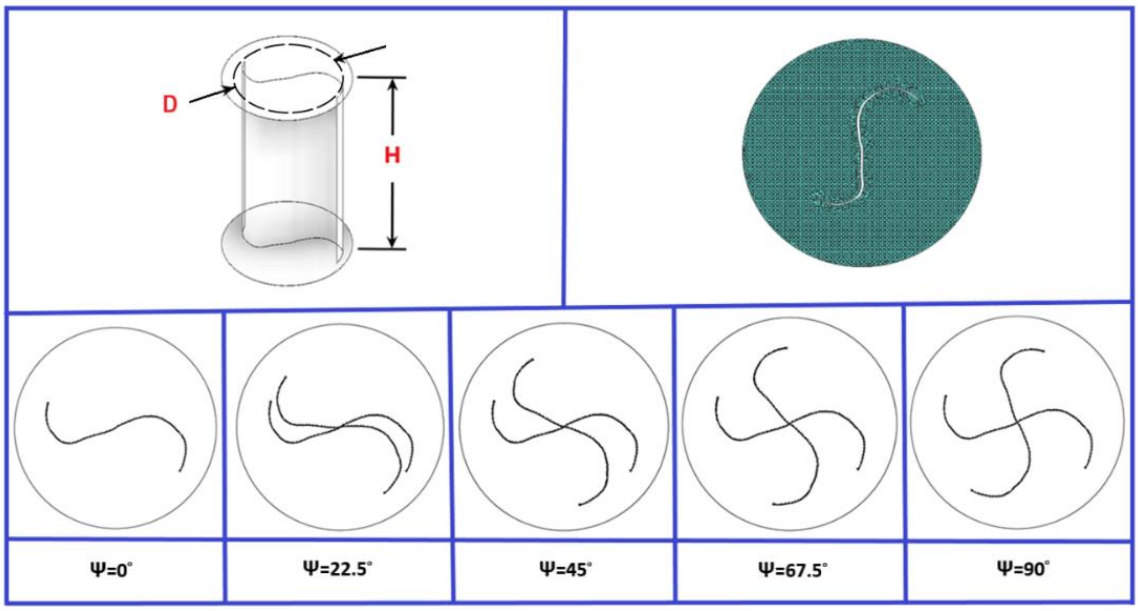

(b) Model 2

Figure 3- The proposed rotor geometries

4. Experimental Setup

This section describes the test section assembly at the Advanced Fluid Mechanics Lab, Faculty of Engineering, Menoufia University. The detailed setup is illustrated in Figures (4-a), (4-b), and (4-c).

Figure (4) shows a layout and photograph of the test rig used in the present work, respectively. It consists mainly of a centrifugal fan (1) with a maximum wind speed of 13 m/s at its exit duct. The fan is driven by an AC motor (2) of 1480 rpm and 15 HP rated power as shown in Figure (4-a). Furthermore, the Ac motor is connected to the fan through belt hoop system for velocity reducing. The diameter ratio is set to be 0.25 which results in reducing the fan rotational speed to be 25% of the AC motor rotational speed. The input voltage to the AC motor is controlled through voltage regulator, as shown in Figure (4-a and c). Varying the input voltage to the AC motor regulates its output rotational speed as required for the considered measurement.

A 1 m^2 circular cross-sectional area duct (3) of 1.5 m length is connected to the fan exit. Screen foam is used to get a uniform distributed flow out of the fan exit duct. The screen is installed just before the square to circular cross section converter in the duct connected to the fan. The duct is fabricated from galvanized iron sheets of thickness 1.5 mm, which is supported by steel bars from outside. The rotor (6) is then placed at center position in front of the duct exit using a structure housing (5) fabricated from mild steel plates. The Savonius rotor projected area facing the wind is (30 cm × 60 cm). The rotor is connected to the steel housing through its upper and lower end plates by a steel shaft (6) of 30 mm diameter.

The wind turbine is placed in an open jet flow, and is subjected to non-uniform wind speed distribution. Hence, it is necessary to obtain the average value of the inflow wind speed hitting the turbine blades. A grid of 144 cells covering the rotor projected area is constructed with a fixed step of 10 cm in each direction, as shown in Figure (4-b). The wind speed facing the rotor is measured horizontally and vertically through the grid points. The average wind speed is calculated considering the area weighted averaged of the measured wind speed values through the projected area of the rotor only. In the measuring experiment, the mean velocity distribution is measured utilizing digital pitot tube while the torque and rotational speed are measured using a torque meter. The digital standard pitot tube (Extech HD350 Pitot Tube Anemometer and Differential Manometer) with resolution of 0.01 m/s, range 0 to 80 m/s, and accuracy of $\pm$ 0.03 is used. Further, the digital torque meter (WinEasyTORK Manual Version 1.0 Model: MO.RT2MTOR. 541.R4) is utilized. The torque meter is a compact digital torque meter with range 0 to 25 N.m and accuracy of 0.001 N.m

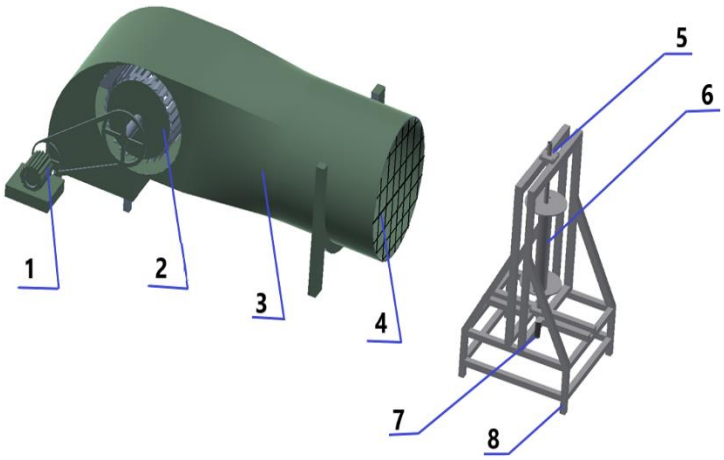

(a) Diagram of the experimental set up

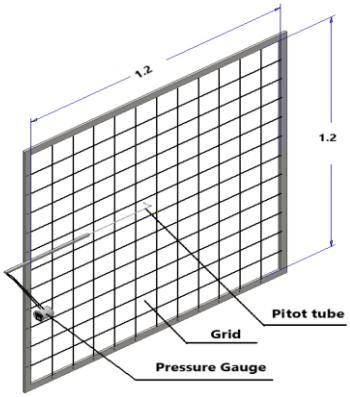

(b) wind speed Measuring grid

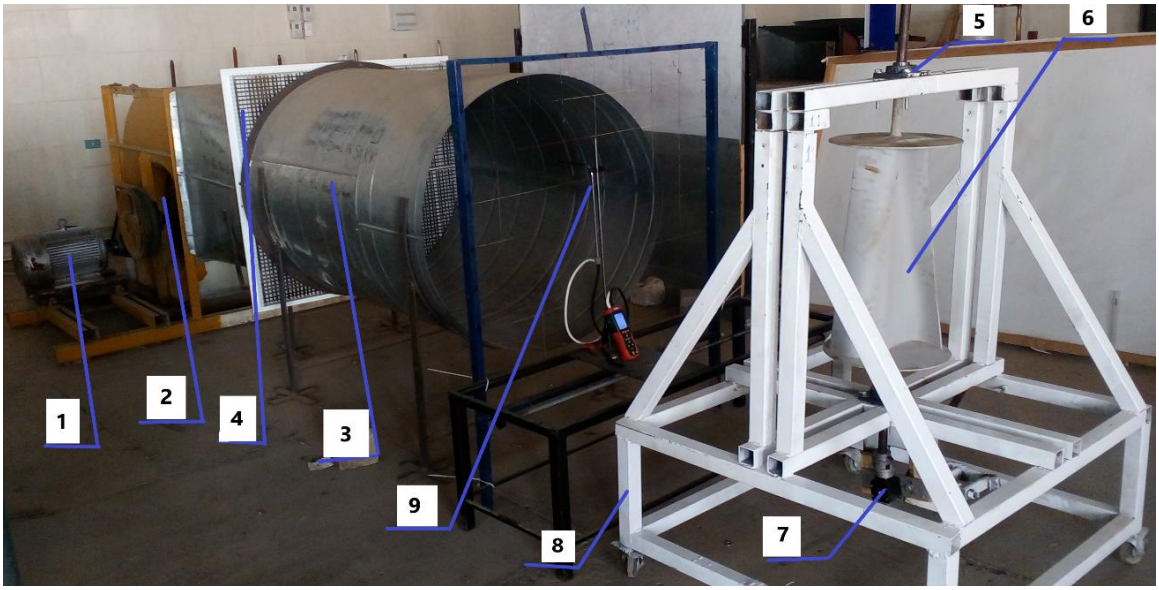

(c) Photograph of the experimental setup assembly

(1) AC motor (2) Centrifugal fan (3) Duct (4) Grid (5) Bearings (6) Rotor (7) Torque meter (8) Frame (9) Pitot tube

Figure 4- The experimental test rig of the present work

5. Results and Discussion

5.1. *Numerical Results*

This section presents the CFD results of the two proposed rotor models presented in section 3. Five equally-steps twist angles ranging from 0° to 90° are investigated. Performance comparisons between the two considered models in terms of power coefficient are illustrated in Figures (5-a to e). Both models achieve peak power coefficient higher than 20% at all twist angles. It is also noted that the two models have almost similar performance except at higher tip speed ratios. Further, Model 1 achieves slightly better performance, as compared to Model 2. The maximum power coefficient C_{Pmax} of the two models is presented in Figure (6). It is noted that twisting the rotor blade provides higher performance. The triggered optimum twist angle for the two models is found to be 45°, beyond this value, the rotor performance slightly reduced. However, Model 1 has a superior performance with 2.28 % higher than Model 2.

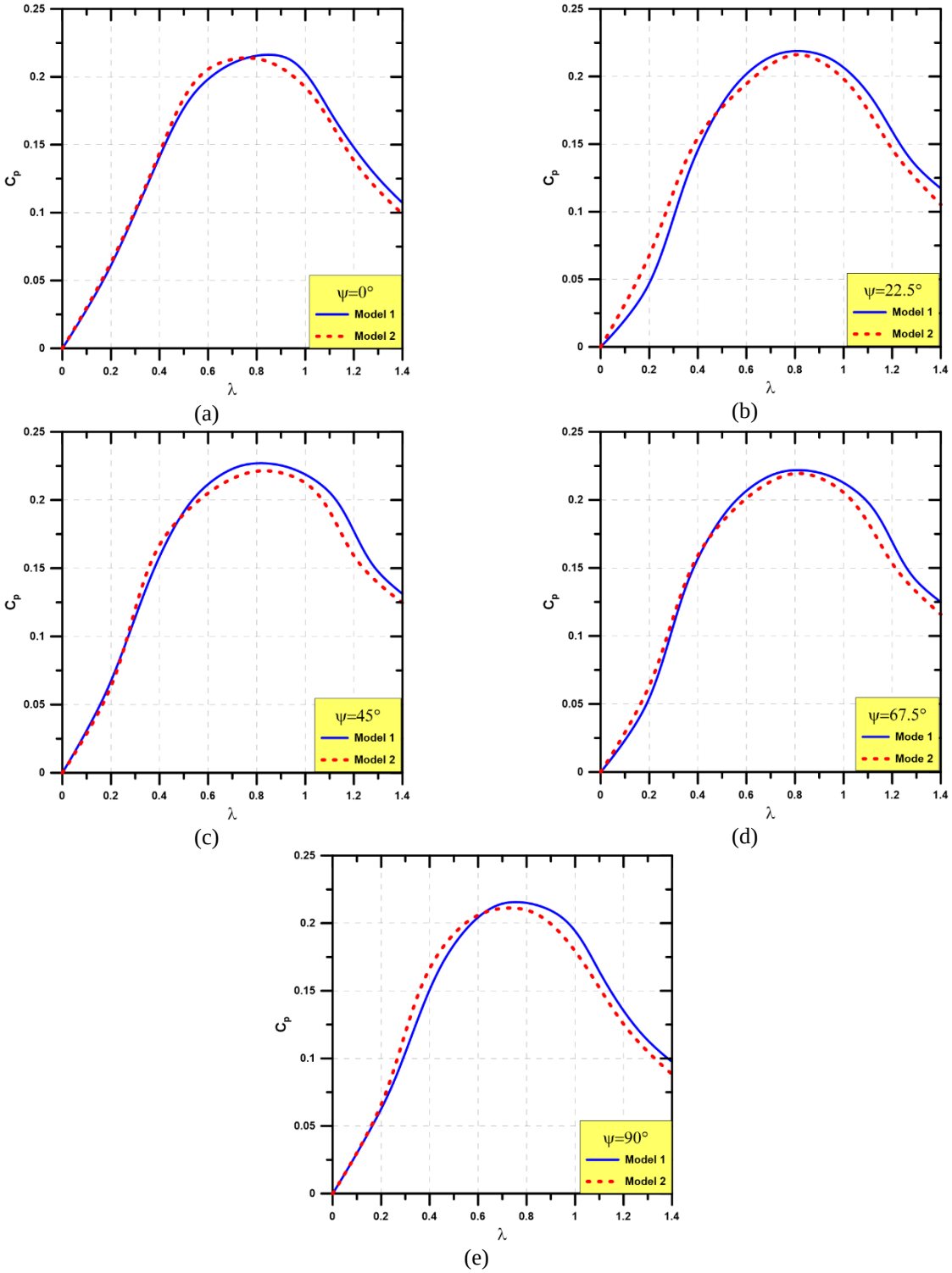

Figure 5- Performance comparison between the proposed models at different twist angles

Figure 7 compares the performance of the present modified rotors with the base rotors reported in [5] and [24]. The performance is significantly higher than the performance of the standard Savonius rotor, as reported in [24]. The percentage increase in Cp_{max} is around 25%. Furthermore, there is a noticeable gain in Cp_{max} of the present models compared to the modified shape presented by [5].

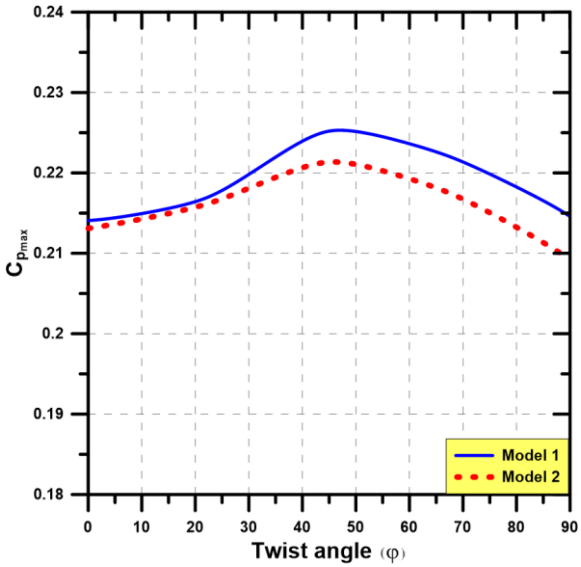

Figure 6- Maximum power coefficient obtained for the two models at different twist angles

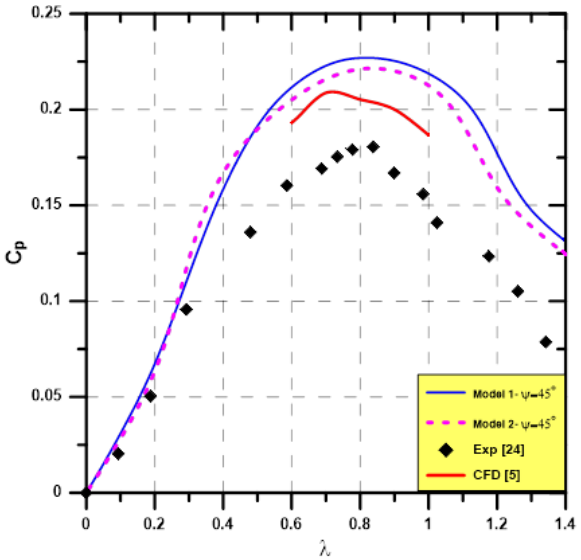

Figure 7- Comparison of Cp for the present modified rotors and the base rotors presented in [5] and [24].

Pressure and velocity contours for both models are illustrated in Figure (8). The pressure shows noticeable variation over the advancing and returning blades at the various rotation angles. This leads to a significant variation in the forces exerted on the rotor blades which affect the variation of rotor torque. The velocity contours present high values in front of the advancing blade. However, at rotation angle of θ=135° the returning blade precedes which extends the velocity reduction over the advancing blade.

The variation of rotor torque in terms of torque coefficient C_T is presented in Figure (9) during one cycle, 360°. It is shown that Model 1 has positive C_T through the complete cycle for all twist angles. However, Model 2 reports partially negative C_T except for ψ=90° which gives positive C_T during the entire operation cycle. The amplitude variation of C_T is further higher for Model 2 as compared to Model 1. It is obvious that, introducing higher twist angles, reduces the cyclic torque variation for both models. It is noted that for Model 1, the reduction in cyclic torque variation is less significant for twist angles beyond 45°. Hence, Model 1 with ψ=45° is considered the best rotor model which will be tested in the present experimental work.

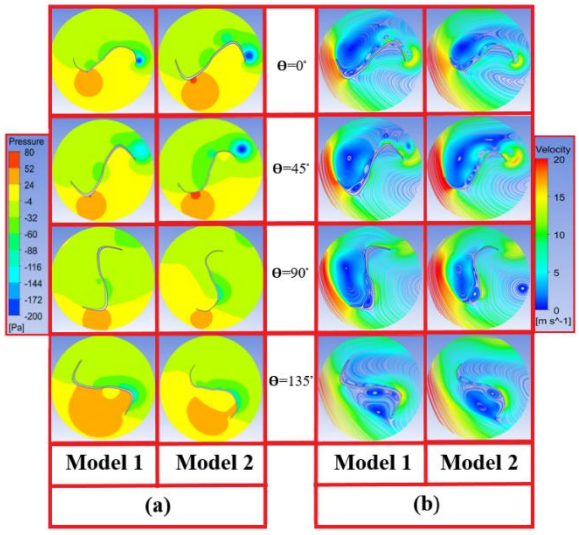

Figure 8- Pressure and velocity contours for the two rotor models at various rotation angles, ψ=45°

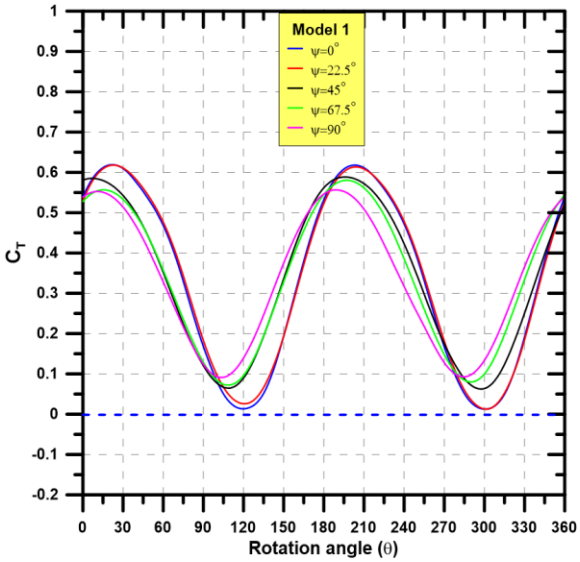

(a)

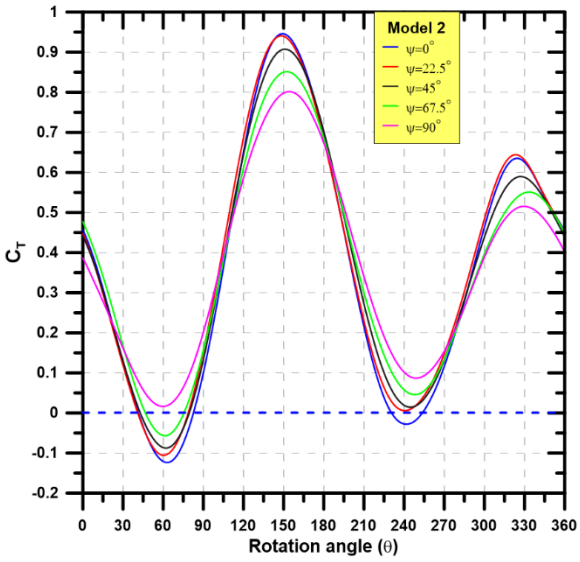

(b)

Figure 9- Torque coefficient obtained for the two models at different twist angles.

5.2. *Experimental Results*

The numerical results presented in the previous section reveal that Model 1 with ψ=45° achieves the highest performance, as compared to other models. Consequently, it is aimed to test the performance of the optimum rotor experimentally. Schematic representation along with a photograph of the fabricated rotor of Model 1 is presented in Figure (10). The rotor blades along with the endplates are fabricated from fiberglass material by casting process. Following that the rotor blades, the endplates, and the shaft are connected together to form the wind turbine measuring system assembly.

The measurements are conducted at various wind speeds of 6, 8, and 10 m/s. Figure (11) introduces performance comparisons between the present experimental and numerical results. There is an acceptable agreement between the numerical and experimental data. However, the deviation increases at higher tip speed ratios. Increasing the inflow wind speed leads to raising the rotor performance. Further, the operating range is expanded for the inflow wind speed of 10 m/s with C_{Pmax}= 0.221. Model 1 proposed in the present investigation is found to operate with higher performance, as obtained by the experimental measurements. The coefficient of correlation "R^2" is used to evaluate the deviation between the numerical and experimental results. The coefficient of correlation is computed from Maindonald and Braun [28] given in Eq. (7).

$$R^2 = 1 - \frac{\sum(\varphi_{exp} - \varphi_{pred})^2}{\sum(\varphi_{exp} - \overline{\varphi}_{exp})^2} \qquad (7)$$

where $\overline{\varphi}_{exp} = \frac{\sum_{i=1}^{n} \varphi_{exp}}{n}$

The coefficient of correlation is found to be 0.882 for the higher velocity, 10 m/s, while it is found to have a value of 0.901 for the medium flow velocity, 8 m/s. Furthermore, the coefficient of correlation has a higher value of 0.916 for the lower wind velocity, 6 m/s.

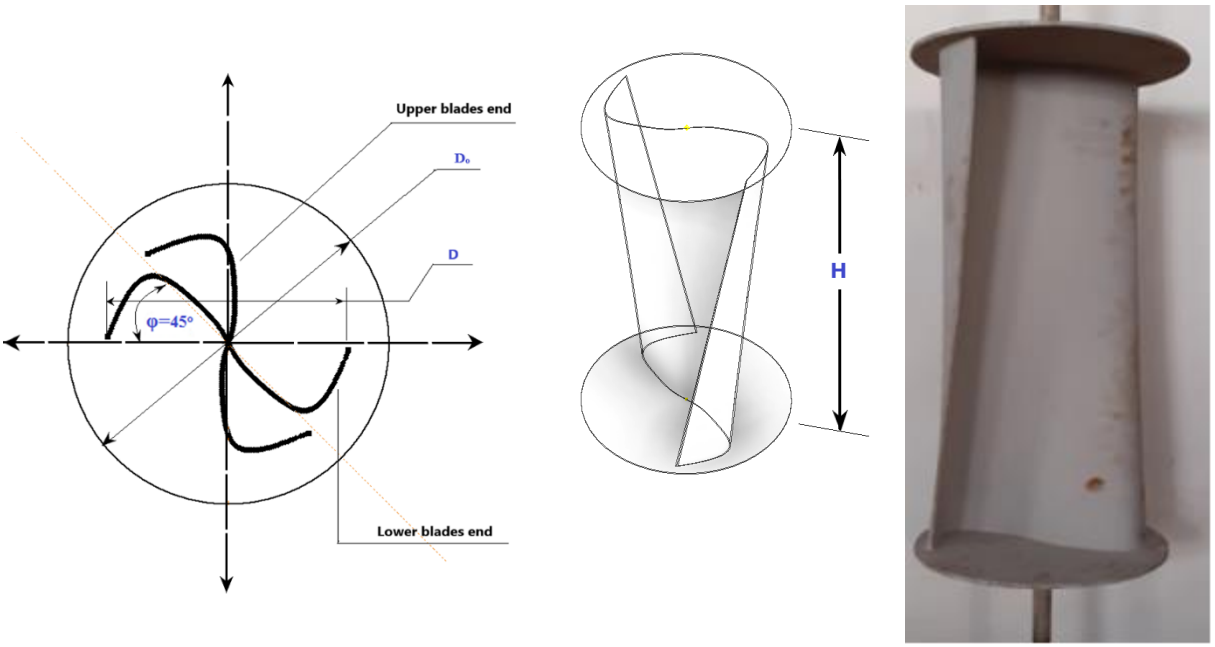

Figure 10- Schematic representation and photograph of Model 1

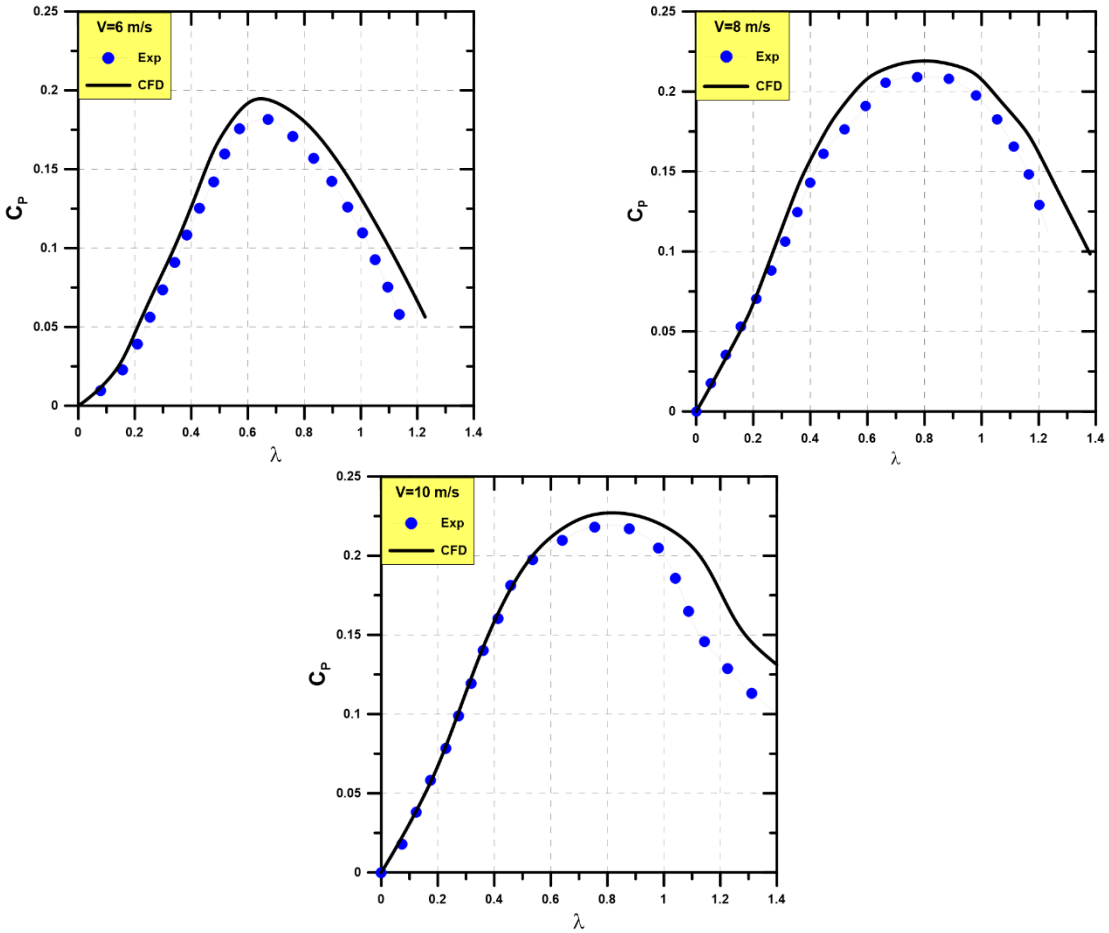

Figure 11- Power coefficient obtained experimentally and numerically at different wind speeds for the optimum model, Model 1

6. Conclusion

This paper presents a numerical and experimental study of two superior Savonius rotor models. Different twist angles were trained for both models. The numerical results revealed that Model 1 with 45^o twist angle has achieved the highest power coefficient. The optimum rotor geometry was further fabricated and tested experimentally at different operating conditions. The experimental results verified the rotor performance obtained by the CFD simulations. It is concluded from the obtained experimental and numerical results that the proposed rotor geometry presented in this work has superior performance. The maximum C_P obtained for the optimum rotor (Model 1) is found to be 0.221 which is significantly higher than the standard Savonius rotor. Furthermore, the results showed reduction in cyclic torque variation of Model 1 which is less significant for twist angles beyond 45°.

7. Acknowledgements

This research work is sponsored by Science & Technology Development Fund (STDF), Egypt, Project ID30140.

8. Nomenclature:

A	Area of wind turbine rotor (m^2)
AR	Aspect ratio
$_pC$	(٢AVρ٠.٥T/(Ω=Power coefficient
$_TC$	(H٦V٦Dρ)/T٤=coefficient Torque
D	(otor diameter (mR
$_oD$	(End plate diameter (m
H	(otor height (mR
T	(Rotor torque (N.m
V	Free stream wind speed (m/s)
δ	Overlap ratio
ρ	(٢Air density (kg/m
Ω	(rad/s) Angular velocity
λ	Tip speed ratio of rotor = Ω D/2V
θ	Rotation angle of the rotor (°)
φ	twist angle (°)

9. References

[1] S. Montelpare, V. D'Alessandro, A. Zoppi, and R. Ricci, "Experimental study on a modified Savonius wind rotor for street lighting systems. Analysis of external appendages and elements", Energy, Vol. 144, 2018, pp. 146-158.

[2] J.V. Akwa, H.A. Vielmo, and A.P. Petry, "A review on the performance of Savonius wind turbines", Renewable and Sustainable Energy Reviews, Vol. 16, 2012, pp. 3054-3064.

[3] M.M. Kamal, and R.P. Saini, "A review on modifications and performance assessment techniques in cross-flow hydrokinetic system", Sustainable Energy Technologies and Assessments, Vol. 51, 2022: 101933.

[4] H. Gad, A.A. Abd El-Hamid, W.A. El-Askary, and M.H. Nasef, "A New Design of Savonius Wind Turbine: Numerical Study", CFD Letters, 6(64), 2014, pp.144-158.

[5] H.A.H. Saeed, A.M.N. Elmekawy, and S.Z. Kassab, "Numerical study of improving Savonius turbine power coefficient by various blade shapes", Alexandria Engineering Journal, Vol. 58, 2019, pp. 429-441.

[6] K. Kacprzak, G. Liskiewicz, and K. Sobczak, "Numerical investigation of conventional and modified Savonius wind Turbines", Renewable Energy, Vol. 60, 2013, pp. 578-585.

[7] M. Al-Ghriybah, M.F. Zulkafli, D.H. Didane, and S. Mohd, "The effect of spacing between inner blades on the performance of the Savonius wind turbine", Sustain Energy Technol Assess, Vol. 43, 2021: 100988.

[8] M. Al-Ghriybah, M.F. Zulkafli, D.H. Didane, and S. Mohd, "The effect of inner blade position on the performance of the Savonius rotor", Sustainable Energy Technology Assessment, Vol. 36, 2019: 100534.

[9] T. Hayashi, Y. Li, and Y. Hara. "Wind tunnel tests on a different phase three-stage Savonius rotor", JSME International Jounal Series B Fluids and Thermal Engineering, Vol. 48, 2005, pp. 9-16.

[10] S. Frikha, Z. Driss, E. Ayadi, Z. Masmoudi, and M.S. Abid. "Numerical and experimental characterization of multi-stage Savonius rotors", Energy, Vol. 114, 2016, pp. 382-404.

[11] N.H. Mahmoud, A.A. El-Haroun, E. Wahba, and M.H. Nasef, "An experimental study on improvement of Savonius rotor performance", Alexanderia Engineering Journal, Vol. 51, 2012, pp. 19-25.

[12] J.V. Akwa , H.A. Vielmo, and A.P. Petry, "A review on the performance of Savonius wind turbines", Renewable and Sustainable Energy Reviews, Vol. 16, 2012, pp. 3054-3064.

[13] M.A. Kamoji, S.B. Kedare, and S.V. Prabhu, "Experimental investigations on single stage, two stage and three stage conventional Savonius rotor", International Journal of Energy Research, 32(10), 2008, pp. 877-895.

[14] J.L. Menet "A double-step Savonius rotor for local production of electricity: a design study", Renewable Energy, Vol. 29, 2004, pp.1843-1862.

[15] A.S. Saad, A. Elwardany, I.I. El-Sharkawy, S.

Ookawara, and M. Ahmed, "Performance evaluation of a novel vertical axis wind turbine using twisted blades in multi-stage Savonius rotors ", Energy Conversion and Management, Vol. 235, 2021: 114013.
[16] J. Kumbernuss, J. Chen, H. Yang, and L. Lu, "Investigation into the relationship of the overlap ratio and shift angle of double stage three bladed vertical axis wind turbine (VAWT)", Journal of Wind Engineering and Industrial Aerodynamics, Vol. 107, 2012, pp. 57-75.
[17] B.A. Bhayo, ad H.H. Al-Kayiem, "Experimental characterization and comparison of performance parameters", Energy, Vol. 138, 2017, pp. 752-763.
[18] A. Damak, Z. Driss, and M.S. Abid, "Optimization of the helical Savonius rotor through wind tunnel experiments", Journal of Wind Engineering and Industrial Aerodynamics, Vol. 174, 2018, pp. 80–93.
[19] K.S. Jeon, J.I. Jeong, J.K. Pan, and K.W. Ryu, "Effects of end plates with various shapes and sizes on helical Savonius wind turbines", Renewable Energy, Vol. 79, 2015, pp. 167–176.
[20] C.P. Oliveira, and A.P. Petry, "Numerical study of a helical Savonius wind turbine", 15th Brazilian Congress of Thermal Sciences and Engineering, ENCIT, Belèm do Parà, (2014).
[21] M.A. Kamoji, S.B. Kedare, and S.V. Prabhu, "Experimental investigations on single stage modified Savonius rotor", Applied Energy, Vol. 86, 2009, pp. 1064-1073.
[22] A. Damak, Z. Driss, M.S. Abid, "Experimental investigation of helical Savonius rotor with a twist of 180", Renewable Energy, Vol. 52, 2013, pp. 136-142.
[23] G.H. Lee, Y.T. Lee, and H. Lim, "Effect of twist angle on the performance of Savonius wind turbine", Renewable Energy, Vol. 89, 2016, pp. 231–244.
[24] W.A. El-Askary, A.S. Saad, A.M. Abdelsalam, I.M. Sakr "Investigating the performance of a twisted modified Savonius rotor", Journal of Wind Engineering and Industrial Aerodynamics, Vol. 182, 2018, pp. 344-355.
[25] A.S. Saad, A.M. AbdelSalam, I.M Sakr, W.A. El-Askary, "Experimental and Numerical Study on a Modified Savonius Rotor", 13th International Conference of Fluid Dynamics (ICFD13), Cairo, Egypt, pp.21-22, (2018).
[26] N. Cuevas-Carvajal, J.S. Cortes-Ramirez, J.A. Norato, C. Hernandez, and M.F. Montoya-Vallejo, "Effect of geometrical parameters on the performance of conventional Savonius VAWT: A review", Renewable and Sustainable Energy Reviews, Vol. 161, 2022, pp. 112314.
[27] W.A. El-Askary, A.S. Saad, A.M. AbdelSalam and I.M. Sakr, "Experimental and theoretical studies for improving the performance of a modified shape Savonius wind turbine", Journal of Energy Resources Technology, Vol. 142, 2020: 121303.
[28] J. Maindonald and W. J. Braun, "Data Analysis and Graphics Using R - An Example-Based Approach" 3rd edition., 2010 (Book).